

# Marker orientation in fiducial registration

Xiaofeng Liu, Hakan Cevikalp, and J. Michael Fitzpatrick

Department of Electrical Engineering and Computer Science  
Vanderbilt University, Nashville, TN 37235

## ABSTRACT

Fiducial markers are often employed in image-guided surgical procedures to provide positional information based on pre-operative images. In the standard technique, centroids of three or more markers are localized in both image space and physical space. The localized positions are used in a closed-form algorithm to determine the three-dimensional rigid-body transformation that will register the two spaces in the least-squares sense. In this work we present (1) a method for determining the orientation of the axis of symmetry of a cylindrical marker in a tomographic image and (2) an extension to the standard approach to rigid-body registration that utilizes the orientation of marker axes as an adjunct to the positions of their centroids. The extension is a closed-form, least-squares solution. Unlike the standard approach, the extension is capable of three-dimensional registration with only two markers. We evaluate the accuracy of the former method by means of CT and MR images of markers attached to a phantom and the accuracy of the latter method by means of computer simulations.

Keywords: Registration, fiducial, marker, rigid body, orientation, image guidance, surgery

## 1. INTRODUCTION

Rigid-body, point-based registration is a standard means for registering two three-dimensional views of a common object when three points are localized in each view. Accurate input points may be obtained by adding fiducial markers to the object and localizing their centroids. Closed-form algorithms for registering point sets have been available since the 1960's and are reviewed in [1]. Unless the markers are spherically symmetric, their orientations, as well as their centroids, can be estimated from their images. Marker orientations can then be used as an adjunct to marker centroids to achieve rigid-body registration.

In this paper we present both a method for determining the orientation of a cylindrical marker and a method for incorporating marker orientation into point-based registration. The latter method is based on an idea published in 1998 Yan *et. al.*, in which the standard point-based method was modified to allow it be applied to the problem of registering images of an object on which was mounted a stereotactic frame [2]. Our method permits three-dimensional registration to be accomplished with two markers and may be the only registration method available when only two markers are available. We test the method for determining marker orientation using CT and MR images. We employ a simulation to estimate the accuracy of the registration method.

## 2. MATERIALS AND METHODS

We acquired MR and CT images of cylindrical markers. Examples are shown in Figure 1. The markers, which are shown photographically in Figure 2, and are designed for use in image-guided surgery<sup>1</sup>, are hollow-plastic, sealed containers whose inner volume is in the shape of a cylinder of height  $5mm$  and diameter  $7mm$ . The inner volume is filled with a fluid that is imagable in both CT and MR [3]. Because the plastic is invisible in MR and is relatively dim in CT in comparison to the fluid, the shape of the marker interior can be segmented and modeled as a cylinder.

### 2.1. Calculation Of marker centroid and orientation

We calculate the orientation of the axis of symmetry of a marker by comparing the marker image with a model of the marker with the following process:

1. Make an initial estimate of the marker's pose:
  - a. Find the centroid of a marker image using intensity weighting [4].
  - b. Perform principal-axis decomposition of the marker image and identify the axis with the largest moment of inertia as the axis of symmetry.
2. Refine the initial estimate by registering the model with the marker image using optical flow [5].

Step 1.b. takes advantage of the fact that the moment of inertia of this marker about its axis of symmetry is significantly different from the moments about its other two principal axes. Optic flow determines an incremental local motion at each point in one image, in this case the model, that will reduce the intensity difference at that point relative to a second image, in this case the actual image. It requires a good starting point, which is provided by initializing the model at the position and orientation determined in the previous steps. Because optic flow is underdetermined [5], it also requires a constraint on the motion, which is easily provided here by imposing rigidity. With rigidity, the solution is over determined, so a rigid motion is chosen that minimizes the total squared difference in intensity over the entire marker. The resulting incremental motion is applied to the model, and the process is repeated until the motion is small. The final direction of the model's axis of symmetry is the calculated marker orientation.

Suppose we have an initial estimate of the marker's localization and orientation. To refine the result, we find the displacement, or the "movement" between the initial estimate and the marker in the given image. Then move the marker from the initial guess by the estimated motion. The object motion can be estimated from image intensity changes in sequential images with optical flow method. Optical flow is based on the assumption that the intensity of the object does not change during the motion. After we get an initial guess of the marker position and orientation, a simulated marker at this position and orientation is generated based on known marker shape model. Then the simulated marker is compared with the real marker in the given image. If the two images are different, the motion between the two images is calculated using optical flow method. The orientation and position of the marker are then updated. These steps are iterated until the motion is sufficiently small.

#### 2.1.1. Initial estimates

After the marker is segmented from the real image, the centroid can be estimated with an intensity weighting method [4]. The marker centroid is calculated as follows:

---

<sup>1</sup> JMF is a consultant for, and has an interest in, Z-Kat, Inc., Hollywood, FL, which markets this marker design under the trademark *Acustar*<sup>TM</sup>.

$$\mathbf{c} = \sum_i (I_i - I_0) \mathbf{v}_i / \sum_i (I_i - I_0) \quad (1)$$

where  $I_i$  is the intensity of the voxel centered at  $\mathbf{v}_i = (\mathbf{v}_x, \mathbf{v}_y, \mathbf{v}_z)$ , and  $I_0$  is the intensity of an empty voxel.

The marker orientation is estimated by calculating its principal axes. One of the three principal axes of a cylinder is the axis of symmetry, which we identify by the unit vector  $\hat{\mathbf{a}}$ ; the other two axes are perpendicular to the principal axis and to each other. After calculating the three principal axes of the marker, we need to identify the axis of symmetry. It is easy to show that, for a cylinder, the second moment about the symmetry axis is  $d^2/8$ , and the moments about the other two axes are each equal to  $h^2/12 + d^2/16$ , where  $d$  is the diameter, and  $h$  is the height of the cylinder. For the markers used in this study, the principal moment is equal to  $6.125 \text{ mm}^2$ , which is 19% larger than that of the other two, which equal  $5.146 \text{ mm}^2$ . So, we select the axis with the largest second moment as the estimated axis of symmetry. Experiments show that such a selection nearly always selects correctly among the three axes.

An alternative way to make the choice is for each possible orientation to generate a simulated marker located on the estimated centroid and to compare the difference between the simulated marker and the real marker. The axis with which the simulated marker is the most similar to the real marker is considered as the marker orientation.

### 2.1.2. Marker simulation

After the initial estimates of the orientation and location of the marker have been obtained, a marker image can be simulated at that orientation and location and compared to the actual marker image. By adjusting the orientation and location to find the best fit of the model image to the actual image, we can refine both orientation and location. We simulate the marker as follows: First the voxels that are completely inside the marker are set as the maximum intensity value of marker voxel values in a real image, and voxels completely outside the marker are set to zero. Then, each voxel near the edge of the marker is set to an intermediate intensity  $I$ , where

$$I = \frac{V_{in}}{V} I_{\max} \quad (2)$$

where  $V_{in}$  is the volume of the voxel that lies intersects the marker,  $V$  is the volume of the entire voxel, and  $I_{\max}$  the voxel intensity of the voxel completely inside the marker.

A problem is how to calculate  $V_{in}$ . Because of the complex shape of the intersection of cylinder and voxel, it is difficult to calculate the exact volume of the intersection. So we approximate it with a simpler numerical technique. We divide each voxel into  $m \times n \times p$  subvoxels. We then designate each subvoxel as being inside the cylinder if its centroid is inside the cylinder and outside otherwise. By accumulating the number of subvoxels whose centers are inside the marker divided by the total number  $mnp$  of subvoxels per voxel, we can get a numerical approximation of  $V_{in}/V$  in Eq. (2). The computation time of this method is proportional to the number of subvoxels. So, for example, if  $m = n = p$ , the computation time is of order  $O(n^3)$ . We find that  $m = n = p = 5$  produces an acceptable compromise between efficiency and accuracy. Alternatively we may select  $m$ ,  $n$  and  $p$  so as to make the side of subvoxel equal to a fixed length, for example,  $0.25 \text{ mm}$ .

### 2.1.3. Optical flow registration

Our method is a rigid-body 3D image registration. Given an initial guess of marker location and orientation, we try to register the simulated image with the real marker using optical flow method. The marker orientation and position can be estimated with subvoxel accuracy. Our approach is based on the 3D version of the optical flow equation. Let  $f(x, y, z, t)$  represent the image intensity at pixel position  $(x, y, z)$  and time  $t$ , the 3D optical flow constraint equation is:

$$f_t + f_x x_t + f_y y_t + f_z z_t = f_t + \nabla f \cdot \mathbf{u} = 0 \quad (3)$$

where  $\mathbf{u} = (x_t, y_t, z_t)$  is the velocity, or the transformation between  $f(x, y, z, t)$  and  $f(x, y, z, t + \Delta t)$ . As we only consider rigid-body motion, the motion can be decomposed into a translation and a rotation. When the rotation angles are small, the motion can be approximately rewritten as:

$$\mathbf{u} = R\mathbf{r} + \mathbf{t} \approx \boldsymbol{\theta} \times \mathbf{r} + \mathbf{t} \quad (4)$$

where  $\mathbf{t} = (t_x, t_y, t_z)$  is the translation vector,  $\boldsymbol{\theta} = (\theta_x, \theta_y, \theta_z)$  is the vector of rotation angles around  $x$ ,  $y$  and  $z$  axis respectively, and  $\mathbf{r} = (r_x, r_y, r_z) = \mathbf{x} - \mathbf{x}_0$  is the image position relative some origin  $\mathbf{x}_0$  lying on the axis of rotation. For the  $i$ th voxel  $(x_i, y_i, z_i)$ , Eq. (3) combined with Eq. (4) can be rewritten numerically as:

$$f_{x_i} t_x + f_{y_i} t_y + f_{z_i} t_z + (f_{z_i} r_{y_i} - f_{y_i} r_{z_i}) \theta_x + (f_{x_i} r_{z_i} - f_{z_i} r_{x_i}) \theta_y + (f_{y_i} r_{x_i} - f_{x_i} r_{y_i}) \theta_z = -\Delta f_i \quad (5)$$

For all the  $N$  voxels, we can write Eq. (5) in the matrix form of:

$$A\mathbf{x} = \mathbf{b} \quad (6)$$

where  $A$  is an  $N$  by 6 matrix,  $\mathbf{x} = (t_x, t_y, t_z, \theta_x, \theta_y, \theta_z)$  is the column vector of the rigid-body motion parameters, and  $\mathbf{b}$  is a  $N$  by 1 column vector. The  $i$ th row of  $A$  is:

$$[f_{x_i}, f_{y_i}, f_{z_i}, f_{z_i} r_{y_i} - f_{y_i} r_{z_i}, f_{x_i} r_{z_i} - f_{z_i} r_{x_i}, f_{y_i} r_{x_i} - f_{x_i} r_{y_i}] \quad (7)$$

and the  $i$ th element of  $\mathbf{b}$  is the difference between the intensity of the real marker and the simulated marker at the  $i$ th voxel.

To solve equation (6), we use singular value decomposition (SVD) to get the optimal  $\mathbf{x}$  in the least square sense. After the transformation is estimated, we update the orientation and axis of symmetry of the marker as follows:

$$\begin{aligned} \mathbf{c}_{\text{new}} &= R\mathbf{c}_{\text{old}} + \mathbf{t}, \\ \hat{\mathbf{a}}_{\text{new}} &= R\hat{\mathbf{a}}_{\text{old}}. \end{aligned} \quad (8)$$

The above steps are executed iteratively until the registration parameters are small.

## 2.2. Incorporating marker orientation into registration.

Standard point-based, rigid registration determines the rotation matrix and translation vector that provide the transformation that minimizes the sum of squares of the distances between corresponding points in two spaces. Several closed-form solutions exist and have been carefully studied [1]. In this application, we have available to us, in addition to the set of corresponding points derived from marker centroids, a set of corresponding orientations given by the axis of symmetry of each marker. To incorporate this information into the determination of the transformation, we extend the standard method to accommodate both point pairs and axis pairs by treating each pair of corresponding axes roughly as an additional point pair for the purposes of calculating the rotation. Thus, for  $N_p$  points and  $N_a$  axes the inputs are the  $2(N_p + N_a)$  vectors,

$$\begin{aligned} \mathbf{p}_1, \dots, \mathbf{p}_{N_p}, \hat{\mathbf{a}}_1, \dots, \hat{\mathbf{a}}_{N_a} \\ \mathbf{q}_1, \dots, \mathbf{q}_{N_p}, \hat{\mathbf{b}}_1, \dots, \hat{\mathbf{b}}_{N_a} \end{aligned} \quad (9)$$

where  $\mathbf{p}_i$  and  $\mathbf{q}_i$  represent points and the unit vectors  $\hat{\mathbf{a}}_i$  and  $\hat{\mathbf{b}}_i$  represent axes in the respective spaces. The outputs are one rotation matrix  $\mathbf{R}$  and one translation vector  $\mathbf{t}$ . The transformation then has the form:

$$\begin{aligned} \mathbf{p}'_i &= \mathbf{R}\mathbf{p}_i + \mathbf{t}, \\ \mathbf{a}'_i &= \mathbf{R}\mathbf{a}_i \end{aligned} \quad (10)$$

for  $i = 1, \dots, N_p$ . The standard method requires that at least three noncollinear points be present in each point set. The extended method allows collinear sets and as few as two points as long as at least one of the axes in each space is nonparallel to the line on which the points in that space lie. The situation with two markers is illustrated in Fig. 3. A solution can be obtained with both points plus one or both of the axes.

While any of the closed-form solutions may be employed, we choose the SVD method [1]. As in the standard method the translation is given by the displacement between the weighted means of the two point sets:

$$\mathbf{t} = \bar{\mathbf{q}} - \bar{\mathbf{p}}, \quad (11)$$

where

$$\bar{\mathbf{p}} = \sum w_i^{(p)} \mathbf{p}_i / \sum w_i^{(p)}, \quad \bar{\mathbf{q}} = \sum w_i^{(p)} \mathbf{q}_i / \sum w_i^{(p)}. \quad (12)$$

Then, a cross-covariance matrix is formed,

$$\mathbf{H} = \sum_{i=1}^{N_p} w_i^{(p)} \tilde{\mathbf{p}}_i \tilde{\mathbf{q}}_i^t + \sum_{i=1}^{N_a} w_i^{(a)} \hat{\mathbf{a}}_i \hat{\mathbf{b}}_i^t \quad (13)$$

where

$$\tilde{\mathbf{p}}_i = \mathbf{p}_i - \bar{\mathbf{p}}, \quad \tilde{\mathbf{q}}_i = \mathbf{q}_i - \bar{\mathbf{q}}. \quad (14)$$

The  $w_i^{(p)}$  and  $w_i^{(a)}$  are weights which may be adjusted according to the certainty of the measurements. (Weights in this work are all set to 1.) Singular value decomposition of  $\mathbf{H}$  is effected:  $\mathbf{U}\mathbf{\Lambda}\mathbf{V}^t = \mathbf{H}$ . Finally,  $\mathbf{R} = \mathbf{U}^t \text{diag}(\mathbf{1}, \mathbf{1}, \det(\mathbf{U}\mathbf{V}))\mathbf{V}$ , where “diag” is a diagonal matrix with the indicated elements on the diagonal; “det” means “determinant of”.

It should be noticed that the association of a given axis with a given marker has no effect on the resulting transformation. Thus, the interchange of orientations of, say, markers A and B, while their centroids remain the same, affects neither  $\mathbf{R}$  nor  $\mathbf{t}$ . In fact, the positions of the axes (as opposed to their orientations) have no effect on the transformation.

### 3. RESULTS

Results are presented both for the determination of the orientation of a single marker and for registration based on both points and orientation axes. In the first case, both computer simulations and phantom imaging were employed. In the second case, only computer simulations were employed. In both cases, the accuracy of the respective method is measured. All computer programs were written using Matlab, Version 6 (The Mathworks, Inc.).

### 3.1. Orientation accuracy

We present results from a computer simulation and from phantom imaging. In each case, we consider orientations that are given by a single axis. Axis orientations were measured using the method described in Section 2.1. Convergence was achieved in 20 iterations. To determine the accuracy of the method, we compare the measured axis  $\hat{\mathbf{a}}_M$  with the true axis  $\hat{\mathbf{a}}_T$ . The error that we present is the angle between these two axes. Because the axis is determined from the image of a fiducial marker, we call this error the *Fiducial Angular Error* (FAE). Thus,  $\text{FAE} = \cos^{-1}(\hat{\mathbf{a}}_M \cdot \hat{\mathbf{a}}_T)$ . In keeping with the standard statistics for fiducial measurement errors, we tabulate the root-mean-square (RMS) value of FAE. In all experiments, 20 iterations were sufficient to reach convergence.

In our first experiment, we applied our method to simulated marker images, produced as described in Section 2.1.2, to which we added noise. As described in that section, the marker had a diameter of 7 mm and a height of 5 mm. We first generated a simulated marker with given marker location and orientation using a value of 255 for  $I_{\max}$ . Then, zero-mean Gaussian noise was added to the simulated image. Several levels of noise were employed with the method being applied 100 times on the same image with independent noise patterns to determine an RMS value for FAE. Many noise levels, pixel sizes, and orientations were tried. The method described in Section 2.1 was applied. Table 1 lists representative results.

**Table 1. RMS for FAE for simulated marker. Pixel size is 1×1×2 mm.**

Signal to Noise Ratio	255/4	255/6	255/8
RMS FAE (degrees)	0.927764	1.91489	2.311613

In our second experiment, we applied the method to markers attached to a multi-tiered plastic phantom with markers attached to each tier. (The phantom is described in [3].) The phantom design permits us to estimate the orientation of each marker by relating it to the location of the centroids of other markers. The phantom was scanned in both MR (Spin-Echo, TR= 3sec, TE=14ms) and CT (kvP=120, exposure=350mas). The MR image had 256×256×59 voxels. Three CT images were acquired. The first had 512×512×44 voxels. The remaining two scans had 512×512×45 voxels. Pixel sizes, slice thicknesses, number of markers and the resulting RMS FAE are given in Table 2.

**Table 2. RMS for FAE for markers imaged on phantom.**

Image Modality	Pixel Size	Slice Thickness	Numb. Markers	RMS FAE (deg)
CT	0.59 mm	2.5 mm	23	2.8
CT (two scans)	0.59 mm	2.0 mm	16 (8 per scan)	4.8
MR	0.94 mm	4.0 mm	15	3.6

### 3.2. Registration accuracy

A simulation was performed to assess the behavior of the registration method described in Section 2.2. Two markers were configured 100mm apart, as shown in Fig. 3, with varying values of the angle  $\theta$ . Thus, the configuration is described by Eq. (9) with  $N_p = 2$  and  $N_a = 2$ . Random, independent, normally distributed perturbations were applied to both centroids and to both axes to produce Point-set 1,  $\mathbf{p}_1, \mathbf{p}_2, \hat{\mathbf{a}}_1, \hat{\mathbf{a}}_2$ . The process was repeated to form Point-set 2:  $\mathbf{q}_1, \mathbf{q}_2, \hat{\mathbf{b}}_1, \hat{\mathbf{b}}_2$ . The two point sets were then registered. The resulting rigid transformation was applied to the target point,  $\mathbf{p}_T$ . We call the magnitude,  $|\mathbf{R}\mathbf{p}_T + \mathbf{t} - \mathbf{p}_T|$ , of its displacement the “target registration error” (TRE) at that point. The point perturbations were applied independently to each coordinate of each point. The RMS perturbation distance is called the *Fiducial Localization Error* (FLE).

Experiments were performed (not shown) with varying values of fiducial localization error  $FLE_1$  and  $FLE_2$ , respectively, in the two space. While the resulting value of TRE was observed, as expected, to depend on the combined  $FLE = (FLE_1^2 + FLE_2^2)^{1/2}$  and  $FAE = (FAE_1^2 + FAE_2^2)^{1/2}$ , it did not depend on the individual values of  $FLE_1$  and  $FLE_2$ . We then set FLE at 1 mm and varied FAE from 1 to 7 degrees. For simplicity we kept the axes in the  $x$ - $y$  plane and we kept the angles of the two marker axes relative to the line between the two marker centroids equal. We varied this angle, which is labeled  $\theta$  in Figure 3, from 10 degrees to 90 degrees. A total of 10,000 repetitions were performed for each combination of FAE and  $\theta$ . The resulting RMS values of TRE are plotted in Fig. 4.

For comparison, TRE was calculated without using marker orientation. Instead, a third marker was located on the  $y$  axis at varying positions three of which are marked by the  $\times$ s in Fig. 3. As the position of that third marker was reduced from 25 to 10 to 5 mm from the center of the first two markers, the value of RMS TRE was calculated [6] and found to increase from 1.4 to 3.4 to 6.9 mm. Not surprisingly, as the three markers become more collinear, the quality of the registration is degraded and the use of two markers with marker orientation becomes relatively more beneficial.

#### 4. DISCUSSION

Registration based on fiducial markers can produce highly accurate results simply by measuring the centroids of three or more markers and bringing them into alignment. When the markers are nonspherical, additional information about their orientation may be obtained that may serve as an adjunct to the centroid positions. In the case of cylindrical markers, the axis of symmetry of the marker provides such information. Accurate measurement of the orientation of that axis is made difficult by the typically small size of the marker relative to the voxel sizes and by noise present in the typical MR or CT image. Nevertheless, as shown in Table 2, we have found that it is possible, for at least one type of cylindrical marker, to estimate the direction of the axis to within about 3 to 5 degrees (RMS values of FAE) in these modalities.

Employing the additional orientation information for the purpose of rigid registration requires an extension of the standard methods, which employ only centroid information. We have shown that a simple extension results in a closed-form solution. One clear advantage of the technique is that it is capable of producing a registration with only two markers, as opposed to a minimum of three. Investigating that case in particular, we have found, as shown by Figure 4, that for a combined FLE of 1 mm and a combined FAE ranging from 1 to 7 degrees, the configuration shown in Figure 3 yields TRE values ranging from 0.9mm to 3.4mm for reasonable values of  $\theta$ . The consistent improvement as  $\theta$  is increased toward 90 degrees is predictable. The orientations of the marker axes provide information about the relative rotation of the two spaces about all axes except themselves, and that information is more accurate for axes that are more perpendicular to the marker axes. The combination of the two marker centroids, on the other hand, provides rotational information about all axes except the  $x$ -axis, and that information is more accurate for axes that are more perpendicular to the  $x$ -axis. Thus, as the marker axes become more perpendicular to the  $x$ -axis, their contributions to orientation information become more complementary to the information provided by the two centroids. It is therefore clear that  $\theta$  should be as close as possible to 90 degrees, but our results show that degradation is minor down to about 70 degrees.

Calculation of the combined RMS FAE,  $FAE = (FAE_1^2 + FAE_2^2)^{1/2}$ , from all combinations of the values given in Table 2 produces values ranging from 4.0 to 6.8 degrees. Thus, the RMS FAE values used in Figure 4 bracket the values of the combined FAE involving these markers and these modalities (i.e., CT-CT, CT-MR, and MR-MR). These values of TRE are comparable to that achievable with three markers when the markers are configured such that the target is outside the triangle formed by the markers, as in Figure 3 and becomes more important as the marker configuration

becomes more collinear. This situation may be important for certain applications when orientation information is available and there are restrictions on the placement of the markers relative to the targets of interest; it is clearly important when only two markers are available and when the markers are nearly collinear.

## 5. CONCLUSION

These results are preliminary, but they show that it is possible to determine the orientations of axis of symmetry of cylindrical markers in CT and MR images to within about 3 to 5 degrees and to use those orientations in a closed-form registration algorithm to achieve a target registration errors of about 2 to 3 millimeters for a configuration in which two markers are separated by 100 mm with a target 50 mm from their mean position. Further work is needed to explore the effects of variations of marker numbers, configurations, axes orientation, and altering marker shape. A larger ratio of height to diameter, for example, might be expected to reduce FAE. While the use of marker orientation unlikely ever to be as effective as the use of additional, widely spaced markers, our results may be important for situations in which only two markers are available or only nearly collinear configurations are feasible.

## 6. REFERENCES

1. J. M. Fitzpatrick, D. L. G. Hill, and C. R. Maurer, Jr. \*, Registration, *Medical Image Processing*, Volume II of the Handbook of Medical Imaging, M. Sonka and J. M. Fitzpatrick, ed., SPIE Press (July, 2000).
2. C. H. Yan, R. T. Whalen, G. S. Beaupre, T. S. Sumanaweera, S. Y. Yen, S. Napel, A new frame-based registration algorithm, *Medical Physics* **25** (1): 121-128 (Jan 1998).
3. C. R. Maurer, Jr., J. M. Fitzpatrick, M. Y. Wang, R. L. Galloway, Jr., R. J. Maciunas, G. S. Allen, Registration of head volume images using implantable fiducial markers, *IEEE Transactions on Medical Imaging* **16** , 447-462 (Aug 1997).
4. M. Y. Wang, C. R. Maurer, Jr., J. M. Fitzpatrick, and R. J. Maciunas, An automatic technique for finding and localizing externally attached markers in CT and MR volume images of the head, *IEEE Transactions on Biomedical Engineering* **43**, 627-637 (Jun 1996).
5. M. Y. Wang, *Fiducial Marker Recognition and Localization for Image-Guided surgery Using Point-Based Registration*, Ph.D. Dissertation, Computer Science, Vanderbilt University, Nashville, TN (May 1998).
6. J. M. Fitzpatrick, J. B. West, C. R. Maruer, Jr., Predicting error in rigid-body, point-based image registration, *IEEE Transactions on Medical Imaging* **17**, 694-702 (Oct 1998).

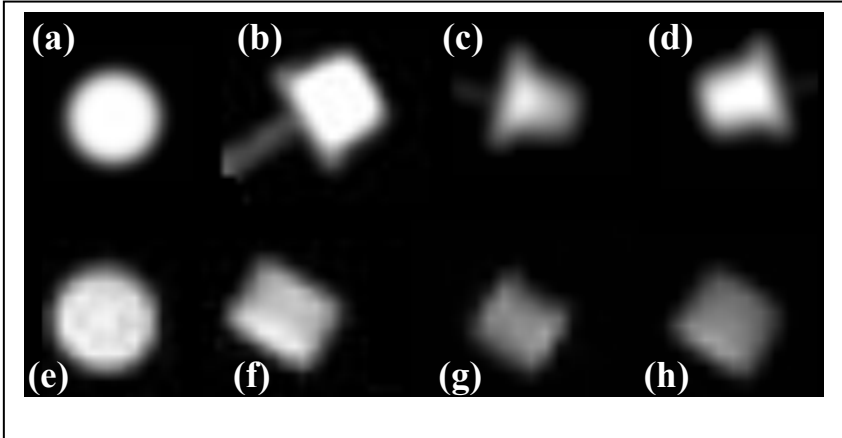


**Figure 1.** CT and MR images of markers. (a)-(d) are CT. (e)-(h) are MR. Note that the plastic container is relatively dim in CT and is invisible in MR. By proper thresholding it is possible to segment the interior in CT before calculating the centroid and axis of symmetry. In MR voxel sizes are larger and noise levels are higher, so the image is of somewhat lower quality.

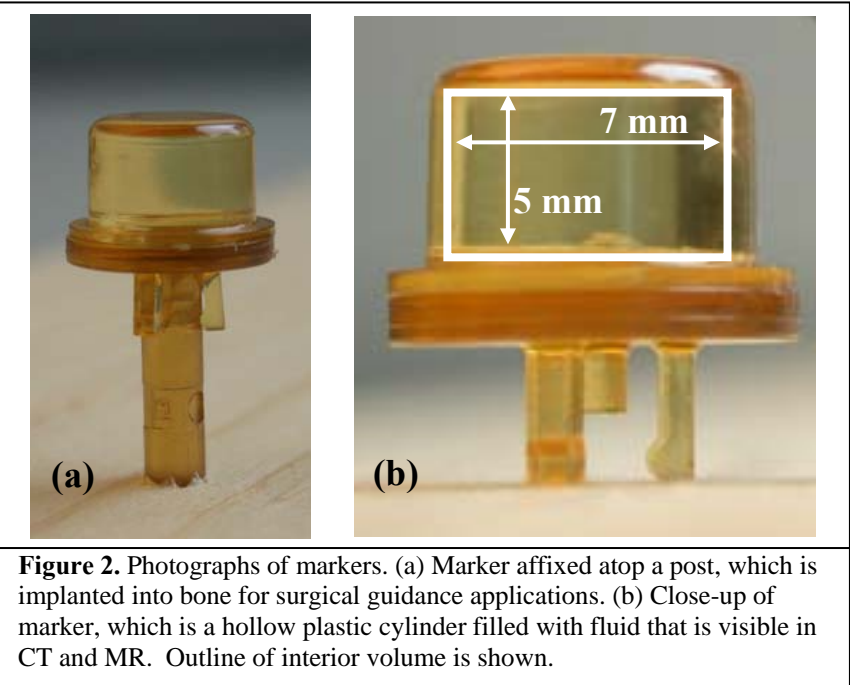


**Figure 2.** Photographs of markers. (a) Marker affixed atop a post, which is implanted into bone for surgical guidance applications. (b) Close-up of marker, which is a hollow plastic cylinder filled with fluid that is visible in CT and MR. Outline of interior volume is shown.

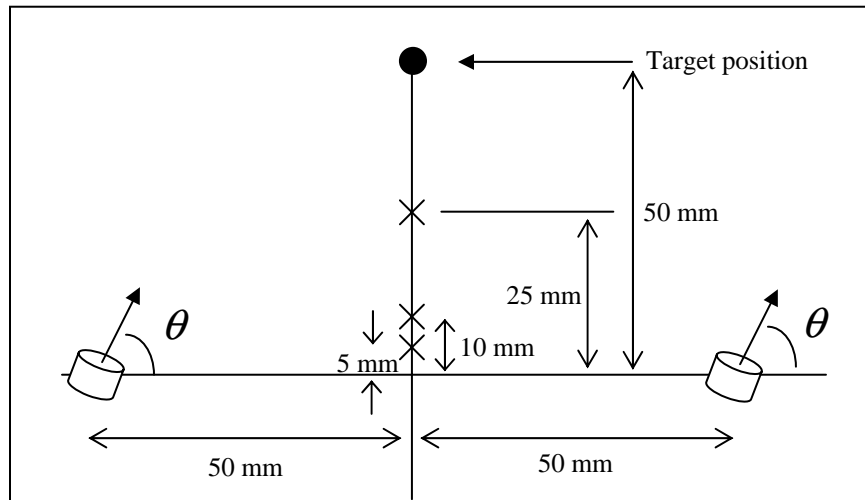


**Figure 3.** Marker Configuration used in our testing. Two cylindrical markers with nominal angular orientations  $\theta$  are located at  $[x,y,z] = [-50,0,0]$  and  $[+50,0,0]$ . The Xs show positions of a third marker, as described in the text.

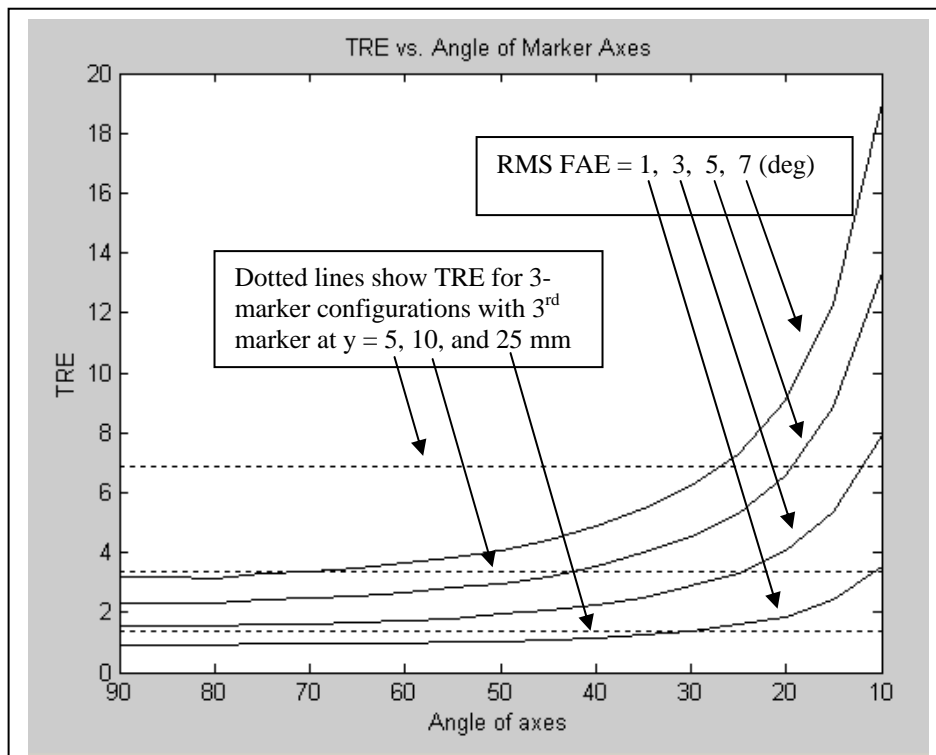


**Figure 4.** Plots of Target registration error (TRE) versus  $\theta$  for the marker configuration of Figure 3 for fiducial angular error (RMS FAE) of 1, 3, 5, and 7 degrees. Larger values of FAE correspond to higher plots. The dotted lines show TRE for the three-marker configurations shown in Figure 3 with higher lines corresponding to positions of the third marker that are closer to the x-axis.